Colloid & Polymer Science Colloid Polym Sci 267:687-701 (1989)

SAXS investigation on the influence of oil dilution on morphological changes in a SBS block copolymer during the first draw cycle

N. Stribeck, P. Bösecke, and S. Polizzi[1])

Institut für Technische und Makromolekulare Chemie der Universität Hamburg, Hamburg, F.R.G.
[1]) Dipartimento di Chimica Fisica, Università degli Studi di Venezia, Venezia, Italy

Abstract: Spin-cast films of one pure SBS and two oil-extended SBS samples were observed during first cycle drawing in the synchrotron radiation beam at Hasylab. For evaluation, from a two-dimensional Vidicon scattering picture the scattering curve was extracted by intersecting perpendicular to the observed layer lines. Using a method described in a preceding paper [1], the scattering curve is analyzed by fitting to one-dimensional two-phase models. Essential for a fit with parameters of physical sense is the assumption of at least two components. One of these two main components is identified with fibrils containing PS cylinders, the axes of which are orientated parallel; the other is identified with fibrils containing cylinders transverse to the drawing direction.

For the mechanical properties of the thermoplastic rubber this splitting of cylinder orientation in the drawn state seems to be of some importance. Only the cylinders of the longitudinal component turn out to be rigid, while the cylinders of the transversal component appear to yield and even break.

The amount of cylinders allotted to each of the two components in the drawn state varies as a function of the diluent. An extrapolation of topological parameters back to the undrawn state indicates a possible reason, a fair variation of the cylindrical particle dimensions within a "lattice cell" of only slighly varying dimensions. While paraffinic mineral oil dilution causes the cylinders lengths to decrease, thus improving cylinder orientability within the pseudo lattice cell, aromatic oil dilution increases the particles diameters.

A remaining faint contribution to the scattering pattern that produces the layer lines is suggested not to be caused by a periodic structure, but by a single and precisely defined polybutadiene matrix length ("string") between two PS cylinders with a considerable height variance.

Key words: SAXS, orientated fibrils, block copolymers, drawing, synchrotron radiation.

1. Introduction

The rubbery nature of styrene-butadiene-styrene (SBS) block copolymers with low polystyrene (PS) content is an effect of the known microphase separation, causing the PS phase to form particles of various shape within a polybutadiene (PB) matrix. At room temperature the PS particles fix the ends of PB chains at their surface – thus the thermoplastic rubber represents a physical network.

Since it is obvious that the morphology of the two-phase system will determine the elastic behavior of the rubber, many authors have studied the morphology of undrawn samples using electron microscopy (EM) and small angle x-ray scattering (SAXS). To acquire deeper knowledge on structure and properties of the thermoplastic rubber, SAXS is a tool that even allows studies in the elongated state.

Early in 1967, Hendus et al. [2] observed an originally isotropic scattering pattern from an SBS sample, which deforms under strain towards "a very narrow ellipse with an intensity accumulation of layer line character". They described an inexplicably high periodicity of about 900 nm computed from the distances between the layer line reflections. Three papers recently published on the subject of strained thermoplastic rubbers are known to us. Séguéla and Prud'-

homme [3] studied films of a commercial SBS product that were slowly cast from the solvent at room temperature. This procedure is known to yield a perfect microstructure and seems to be a reason for their observation of a rather detailed scattering pattern of a four-point-diagram kind (in the present paper we deal with sample films produced in a rapid spin-casting process, far from equilibrium, and our samples appear more like the ones from the early study of Hendus et al.). The second work known to us and recently published is that of Pakula et al. [4]. The authors used commercial products as well, but part of the samples were prepared by press molding under shear flow, the others were prepared in a way similar to that of Séguéla and Prud'homme. For interpretation Pakula et al. developed a model of an unidimensional lattice of cylindrical microdomains, where changes of cylinder orientation do not play a predominant role. By comparison, between model and scattering patterns they drew conclusions about different processes for structural changes caused by deformation. As have other authors, they suggest a yielding and fragmentation process of long cylinders orientated transverse to the direction of strain.

A third paper was published recently [5], based on time-resolved SAXS measurements with a linear detector and synchrotron radiation on SBS block copolymer films from a solvent casting process. The experimental method is similar to the one used by us in the present work, but the authors, Richards and Mullin, described the development of peak reflections as a function of stress and elongation in a more phenomenological way. These authors found that under stretching up to an elongation of 10 the cylindrical particles remain unchanged. They stated the hypothesis that under uniaxial extension the cylindrical domains are partially aligned parallel to the applied stress.

Blending of SBS block copolymers with typically 50 pph (parts per hundred parts of polymer) of a mineral oil fraction is of technical interest since it is known to improve tensile strength of the product and processing capabilities [6]. This improvement cannot be reached by the use of highly aromatic mineral oil fractions, so normally a light, mainly paraffinic mineral oil fraction is taken. Although there is a lot of patent literature on this topic, we did not find papers on the morphology of oil extended grades of SBS copolymers except the ones of Ceausescu, Bordeianu et al. [7, 8]. These authors, by use of rubber network theories, indirectly conclude that the PS particles in the sample diluted with 50 pph of paraffinic mineral oil should be closer to spherical shape than the ones in the undiluted sample. Together with that group we recently worked out an SAXS study on their samples in the unstretched state using the absolute measurement method [9]. We were able to determine the contrast variation between the two phases as a function of the content of various oils in the PB matrix and could show that paraffinic oil dilution improves phase separation. Probably due to the rapid solvent evaporation in the spin-casting process, phase separation in the undiluted sample was found to be rather poor. We were not able to analyze the topology of the two-phase system from the isotropic scattering curves taken with a Kratky camera.

The present work deals with scattering patterns resulting from the drawn state. Experiment, phenomenology, and first interpreting steps are to be published in a separate paper [10]. Due to the more technical process of sample preparation, our samples show a rather simple layer line-pattern (see above). Thus, it appeared promising to develop an adapted theory for the small-angle scattering of orientated cylindrical particles of moderate anisotropy, as was done in a preceding work by one of us [1]. This adapted evaluation method is founded on Rulands theory of interface distribution functions [11]. By use of the new theoretical approach in the present paper the attempt is made to fully describe the scattering curve of the samples in the direction perpendicular to the layer lines and thus reveal the morphology of the samples as a function of elongation and diluting agent.

2. Theoretical

2.1 Fibrils containing orientated particles of moderate anisotropy

The evaluations in this paper are based on the model of a two-phase system, the particles of which are organized in highly orientated fibrils, as was proposed in a preceding work (Stribeck [1]). Essential for this model is the assumption that the smaller particles, forming one of the phases, are of moderate anisotropy only. Those particles shall be approximated by cylinders. If the observable scattering pattern just covers the region inside the first zeros of the cylinders structural factor, a section through the scattering pattern in the direction of the fibrillar axes is approximately proportional to the scattering curve of the one-dimensional fibril, even in the case that orientation is not really perfect.

The basic equation for the one-dimensional model of the fibril was given as Eq. 13 of [1]:

$$I_1(s_3) = A_p/s_3^2 \cdot [1 - \sum_i w_i H_i(s_3)]$$

$$H_i(s_3) = \cos(2\pi d_i s_3) \cdot \exp(-2\pi^2 \sigma_i^2 s_3^2) \quad (1)$$

with A_p being the asymptote of the one-dimensional Porod law. $H_i(s_3)$ is the Fourier transform of the i-th distance distribution, according to Rulands theory [11]. $H_i(s_3)$ describes the modulation of the scattering pattern due to the distance d_i between any chosen phase boundary (interface) within the fibril and its i-th neighbor. In this equation σ_i denotes the variance of the distance d_i due to its variations along the fibril and over the whole ensemble in the irradiated volume.

The parameters w_i (integer numbers, taking into account the multiplicity and sign of the H_i) and d_i describe the general model of the one-dimensional structure. If one decides on the number and succession of basic distinguishable heights in the one-dimensional structure, all the w_i are given and the d_i can be reduced to those basic heights (e. g., $d_1 = h_c$, the mean height of the cylinders, and $d_2 = h_g$, the mean height of the gaps in the fibril).

An additional assumption in the statistical model about the cylinders' arrangement within the fibrils and/or within the irradiated volume will reduce the series of independent σ_i-parameters to a number of basic variances (e. g., $\sigma_1 = \sigma_c$ and $\sigma_2 = \sigma_g$, the variances of the cylinder heights and those of the gaps in between).

The above Eq. (1) is very general. It describes the scattering of finite fibrils if the summation is extended over a finite number of summands only; it can deal with any number of distinguishable basic heights in the fibril; it can be superposed, if a multi-component system is assumed.

In [1] it was shown how Eq. (1) can serve as a tool for stepwise model confinement: if one allows a free-running set of many σ_i-parameters, the assumed model can be checked for physical sense. Either the set of σ_i indicates a fibrillar statistics of physical sense (which in this case can be assumed to be valid, reducing the parameter set), or it does not (in which case the general fibrillar model should be revised). This feedback procedure led to the discussion of fibrils with more than two basic heights and to the introduction of "strings". A string component shall be defined as an ensemble of finite fibrils with only two cylindrical heads of poor definition (i. e., great variance σ_c) and a well-defined gap length in between.

In supplement to the cited previous work, A_p, the Porod asymptote shall be discussed in detail.

2.2 The Porod asymptote for single cylinders

Firstly, the scattering of single cylinders is discussed. Generalizing Eq. (7) in [1] for the case of any electron density difference $\Delta\varrho_{el}$ between cylinder and matrix, the single cylinders scattering intensity $I_c(\vec{s})$ is given by

$$I_c(\vec{s}) = \Delta\varrho_{el}^2 \cdot V_c^2 \cdot \mathrm{Jinc}^2(\pi d_c s_{12}) \cdot \mathrm{sinc}^2(\pi h_c s_3) \quad (2)$$

with V_c being the cylinder volume and d_c its diameter. Jinc(x) shall be defined as $\mathrm{Jinc}(x) = 2 \cdot J_1(x)/x$, with $J_1(x)$ being the Bessel function of first kind and first order. sinc(x) is defined as $\mathrm{sinc}(x) = \sin(x)/x$. $\vec{s}$ is the scattering vetor, s_{12} and s_3 its radial and axial components in cylinder coordinates and $s = |\vec{s}| = 2/\lambda_w \cdot \sin\theta$. Here λ_w is the wavelength of the radiation and θ the half of the scattering angle.

Regarding the offset axial section through the scattering pattern of $I_c(\vec{s})$ at the place s'_{12} and the trigonometrical equivalence $\sin^2\alpha = (1 - \cos 2\alpha)/2$ we get

$$[I_c(\vec{s})]_{s'_{12}}(s_3) = A_p/s_3^2 \cdot [1 - \cos(2\pi h_c s_3)] \quad (3)$$

with

$$A_p = \frac{\Delta\varrho_{el}^2 \cdot S_{cl}^2}{2\pi^2} \cdot \mathrm{Jinc}^2(\pi d_c s'_{12}) \quad (4)$$

where S_{cl} is the surface of the cylinder lid.

For a system containing many identical cylinders of approximately the same orientation, the weight A_p is given by

$$A_p = n \cdot \frac{\Delta\varrho_{el}^2 \cdot S_{cl}^2}{2\pi^2} \cdot \mathrm{Jinc}^2(\pi d_c s'_{12}) \quad (5)$$

where n is the number of cylinders in the irradiated volume which are sufficiently orientated to meet the model.

The discussion of Eq. (20) in [1] showed that A_p from the single cylinder scattering is equal to that of the fibrillar model in the limiting case of the fibril containing a single cylinder – a result that shall be generalized in the following.

2.3 *The Porod asymptote for fibrils*

For a one-dimensional system, Ruland ([11], p. 419) derived an expression for the Porod asymptote A_p. If in that derivation one takes into account the radial extension of the cylinders and the term of the fibrillar scattering due to an offset axial section ($s'_{12} \neq 0$) one gets

$$A_p = n_f \cdot \frac{k_a}{2\pi^2 \cdot d_p} \cdot \mathrm{Jinc}^2(\pi d_c s'_{12}) \tag{6}$$

with n_f being the number of fibrils in the irradiated volume k_a, the axial equivalent to the Porod invariant (scattering power) and d_p, the one-dimensional average chord length parameter:

$$k_a = \Delta\varrho_{el}^2 \cdot S_{cl}^2 \cdot t \cdot v_c \cdot (1 - v_c)$$

$$\frac{1}{d_p} = \frac{1}{h_c} + \frac{1}{h_g} \tag{7}$$

where t denotes the length of the whole fibril and v_c the volume fraction of the cylinders with respect to the volume of the fibril. Two general simplifications of Eqs. (6, 7) can easily be shown: $(1 - v_c)/d_p = 1/h_c$ and $t \cdot v_c = n_{cf} \cdot h_c$ (the number of cylinders per fibril times the cylinder height). It follows that Eqs. (5 and 6) are identical. Thus, the axial Porod asymptote A_p of a fibrillar system is not affected by the correlations among the particles in the fibril. It simply reflects the nature of individual cylinders on the background of the matrix material. This result is analogous to the isotropic case in which the influence of the two-phase systems topology on the value of A_p is given by the inner surface only.

Discussing Eq. (5) one finds that changes of A_p can either be due to orientation effects (mainly influencing n), variations of the contrast $\Delta\varrho$, or to variations of cylinder dimensions due to deformation. Considering low elongations, the main effect should be given by orientating the cylinders. A change of contrast could raise from matrix density variations (if oil and matrix do not have the same electron density, resulting in a mean density, and the oil is dislocated from the fibrils) or disruption of cylinders and/or matrix at very high elongations. At elongations a little lower the cylinders may act elastically and thus change their dimensions. In this case it seems appropriate to assume conservation of the cylinders excess mass and write Eq. (4) in the form

$$A_p = \frac{\Delta N_{el}^2}{2\pi^2 h_c^2} \cdot \mathrm{Jinc}^2(\pi d_c s'_{12}) \tag{4}$$

with ΔN_{el} being the number of excess electrons, contributing to the individual cylinder. As one can see, a decrease of A_p due to increasing h_c may partly be compensated by the increased of the Jinc-term with decreasing d_c, if s'_{12} were not chosen to be zero.

So, for intermediate macroscopic elongations the weight A_p should be nearly independent from elongation and be proportional to the volume fraction of cylinders meeting the fibrillar model function.

2.4 *Cylinders transverse to stretching direction*

If, under the stretching process, uncorrelated identical cylinders are oriented transverse to the direction of deformation, with their axes laying at random in the plane normal to the direction of strain, their observable scattering intensity $I_{\mathrm{otc}}(s_{12}, s_3)$ is an average over the s_{12}-plane

$$I_{\mathrm{otc}}(s_{12}, s_3) = C \cdot \int_0^{\pi/2} \mathrm{Jinc}^2(\pi d_c u(\varphi, s_{12}, s_3)) \cdot \mathrm{sinc}^2(\pi h_c s_{12} \cdot \sin\varphi) d\varphi \tag{8}$$

with $C = (2/\pi) \cdot n \cdot \Delta\varrho_{el}^2 \cdot V_c^2$ and $u(\varphi, s_{12}, s_3) = \sqrt{(s_{12} \cdot \cos\varphi)^2 + s_3^2}$. For $s_{12} = 0$ the integral is trivial and Eq. 8 yields the known decrease according to the Jinc-term that is caused by the cylinders' radial extension, but now in axial direction of the pattern. For $s_3 = 0$, in radial direction of the pattern, we now get an average between the sinc- and Jinc-terms discussed in [1]. Figure 1 shows the longitudinal (sinc-) and transversal (Jinc-) terms of the orientated cylinders scattering, as well as the averaged decrease in radial direction of the pattern for cylinders orientated transverse to the direction of deformation. The averaged curve is obtained by numerical integration of Eq. (8). The ratio h_c/d_c is chosen to be 2.

If the cylinder dimensions are known, a plot such as that shown in Fig. 1 can help to determine the attenuation factor for the scattering of transversal cylinders in an offset axial section of the scattering pattern. In such a section the shape of the curve in general will be affected as well, and will not reveal the pure Jinc-term that is found for the zero-section. If $s_{12} = s'_{12}$ (the radial offset) is chosen to be a non-zero constant, integration of Eq. (8) allows an estimation of the shape distortion effect due to this non-zero section. Figure 2 shows an

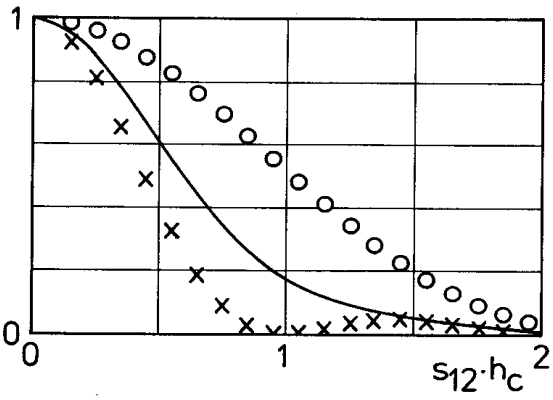

Fig. 1. Cylinders transversal to drawing direction with their axes orientated at random in the normal plane and a h_c/d_c-ratio of 2: Attenuation of averaged particle scattering intensity as a function of the s_{12}-component of scattering vector (perpendicular to drawing direction) compared with the axial (×) and radial (○) scattering term of the cylinders form factor

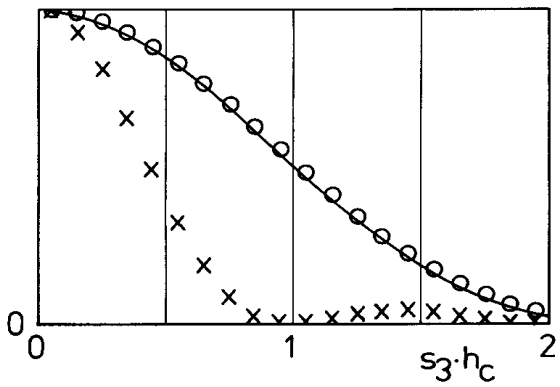

Fig. 2. Cylinders transversal to drawing direction with their axes orientated at random in the normal plane and a h_c/d_c-ratio of 2: Shape of averaged particle scattering curve in an offset section ($s'_{12} = 0.67/h_c$) as a function of the s_3-component of scattering vector (in drawing direction) compared with the axial (×) and radial (○) scattering term of the cylinders form factor

example assuming $s'_{12} = 0.67/h_c$ and $h_c/d_c = 2$. For this parameter set a shape distortion effect can be neglected. Variations of the h_c/d_c-ratio in the range 1 – 10 in further numerical integrations showed negligible distortion as well.

Thus, at least if the relative offset is not greater than in the example tested above, it should be allowed to fit fibrils containing transversal cylinders by the linear model given in [1].

Beyond that, if even within the individual fibrils the transversal cylinders axes are orientated at random (see Fig. 16, middle), their correlated surface normal to the drawing direction S_{cc}, would not significantly differ from that of a fibril in which the cylinders were orientated in longitudinal direction. In this case the attenuation factor due to the offset section and due to the cylinders transversal orientation should not differ from the pure Jinc-term of the longitudinal component, so that the additional attenuation could be approximated by 1 and thus be neglected in the one-dimensional fibrillar scattering model.

3. Experimental

The samples investigated are based on a styrene-butadiene-styrene linear block copolymer with molecular weights $M_n = 80{,}800$ g/mole for the middle and $M_n = 21{,}200$ g/mole for each of the end blocks. This polymer was dissolved in toluene and a film spun cast from the solution thereafter. The resulting sample will be referred to as SBS in the following. Modifications of the pure SBS sample were obtained by additionally dissolving 50 pph (weight parts per hundred parts of the polymer) of a mineral oil fraction in the polymer solution before spin-casting. The sample blended with a highly paraffinic mineral oil fraction shall be referred to as P50, the other blended with a highly aromatic mineral oil fraction shall be named A50.

Synthesis [6] and sample preparation [8] are described elsewhere. The small angle x-ray scattering of the samples was measured at the Hamburg Synchrotron Radiation Laboratory (Hasylab) and recorded with a two-dimensional detector (Vidicon) at a distance of 2.6 m from the sample. The experiment is described in detail in a previous publication on the undiluted sample [10], where scattering patterns, first results, and relaxation phenomena are documented. For each positive and integer-stretching ratio $\lambda = \varepsilon + 1$ a scattering pattern was accumulated for 60 s. When the last scattering pattern was recorded in each of the series, the sample slipped out of the sample holder.

4. Method of data evaluation

Figure 3 shows a contour plot of a typical scattering pattern with the blind spot of the primary beam stop in the center. The cylindrical coordinate system is indicated with s_{12} being its radial and s_3 its axial component. Data for the evaluation procedure were obtained by an axial section through the scattering pattern.

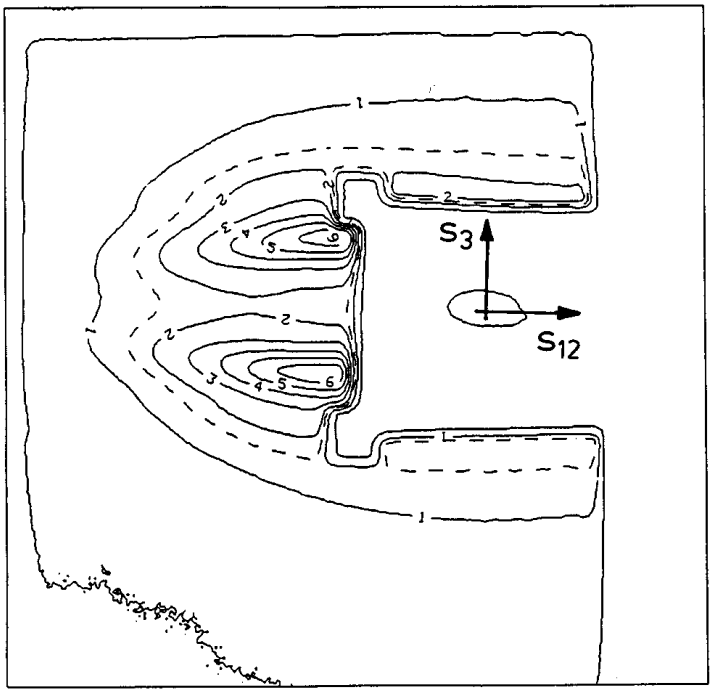

Fig. 3. SAXS-contour plot of an oil-diluted SBS block copolymer sample (33 wt% paraffinic mineral oil, P50) at an elongation of $\varepsilon = 3$

Because of the blind spot the pattern was intersected with a radial offset of $s'_{12} = 0.0176\ \mathrm{nm}^{-1}$ (i. e., just outside the edge of the beam stop). The scattering in the offset section was corrected for actual primary beam luminosity, blind scattering, detector sensitivity, actual absorption coefficient and actual sample thickness [10]. This procedure ensures that all the scattering patterns taken are normalized to the same irradiated volume.

The development of the method of data analysis was described in detail previously [1] and an example of evaluation was given. The mathematical tool used is a Simplex nonlinear regression algorithm on a function $f(s_3) = s_3^2 \cdot [I(\vec{s})]_{s'_{12}}(s_3)$, the intensity data in the section multiplied by the square of the scattering vector. $f(s_3)$ is affinely transformed to ensure good matrix conditioning for the regression procedure by demanding that both ranges of ordinate and abscissa are in the same order of magnitude and close to the middle of a computer real number representation range. Quality of the fit is estimated (after Draper and Smith, [12]) by means of correlation matrix, confidence intervals for each model parameter, residual plot, and the estimated error (E) of the fit, which is defined by

$$E = \sqrt{\frac{\mathrm{RSS}}{m \cdot (m - p)}} \qquad (9)$$

where RSS is the residual sum of squares, m the number of data points, and p the number of parameters.

The regression program is written in Turbo-Pascal 4.0 under MS-DOS, using double-precision real number representation and an arithmetic coprocessor 80287. At a processor frequency of 8 MHz, a regression run with 92 data points and two stacking models takes about 3 h. Addition of two finite-fibril models increases the run-time to about 12 h. For each curve analyzed, the regression tool is used for progressive confinement of the model under the aim to improve the quality of the fit.

The models used for the regression analysis are discussed in detail in [1]. Here only a short review of those important for the discussion shall be given. Known simple models for one-dimensional statistics are based on the assumptions of infinite length of the fibril and two basic mean distances that we name d_1 and d_2 (which may be identified by the height of the cylinder and the height of the gap). Along the fibril the individual distances fluctuate within the range that is given by their variances σ_1 and σ_2. Any composite distance d_i along the fibril will fluctuate with a variance σ_i according to the one-dimensional statistical model that is assumed. The two models important for the later results are stacking statistics and the lattice model. Stacking statistics assume d_1 and d_2 to vary independently. In lattice statistics it is assumed that the lattice constant $d_3 = d_1 + d_2$ is stacked, which makes σ_3 one of the models basic parameters. On the positions defined in this way, the lengths of the kind d_1 are centered. Thus, in this case, d_1, σ_1 and d_3, σ_3 are the parameters basic to the model. One can easily see that stacking statistics have a worse model-inherent long-range order than lattice statistics. Beyond that, both phases in stacking statistics can be principally treated to be of the same kind, while in lattice statistics the phase occupying the places of the lattice is unique, so that watching the error E for both the different lattice model variants will tell which of the two phases is decorating the lattice.

As mentioned in [1], for every elongation and sample all combinations of two parallel infinite fibrillar models are tested. The model combination that proves the smallest estimated error of the fit is taken. Such a model combination fits the general trend of the scattering curve very well, but is not able to describe the higher orders of the layer lines. We will call this model combination the main contribution.

The discussion of the unfitted residual of the main contribution led to the introduction of a subsidiary

contribution of fibrils with finite length, containing just two particles and one gap in between. If the gap is rather well defined, that is $\sigma_2/d_2 \simeq 0$, and the variation of the particle heights over the irradiated volume is rather large, this finite fibril is named a "string" (Fig. 16, right). This model shows the same characteristic modulation of the reflections caused by the well defined gap height that is found in the residual of the main contribution fit.

Finally, main and subsidiary contribution components together are taken to describe the scattering of the elongated SBS samples in the direction of strain.

5. Results and discussion

5.1 General

Comparing the sole main contribution fit with that of the complete model used finally, the fitted parameters of the main contribution are stable, while their intervals of confidence and the interparametric correlations are significantly smaller in the case of the complete model fit. Only the weights A_p are slightly decreased in favor of the subsidiary contribution, if the complete model is chosen.

On the other hand, regression analysis tells that our subsidiary contribution only is a first approximation to a correct description of the layer lines. The intervals of confidence for the parameters occasionally are extremely wide; the interparametric correlations are strong as well. This partly is an effect of the only faint contribution to the scattering curve, yielding inaccuracies due to noise, especially at high values of s_3. But there is a systematic deviation as well. While the single finite-fibril model is able to fit the characteristic modulation of the layer line reflections, it cannot accurately fit the peak positions. If we consider the measured reflections in the residual of the main contribution as a bunch of oscillations, then in the middle of this observed bunch the frequency is higher than for low values of s_3, so that a single finite-fibril model is sometimes not able to follow this behavior. To overcome this, one may superpose a series of such, or try to find a better simple model. The first method is limited by a decrease of evidence and an increase of computing time with increasing number of summands, the latter method by our actual lack of inspiration. An intermediate solution could be found by an assumption of a law that the summands in an assumed series of string components shall follow. In this work up to two of the finite string models are used to describe the higher order layer lines in addition.

The main contribution for both the SBS and the A50 samples is found to be double stacking statistics for all elongations. For the sample P50 diluted with paraffinic oil, this is only true for the elongations $\varepsilon = 1$ and $\varepsilon = 3$. For all the other elongations a double lattice model shows the smallest estimated error of the fit.

In the following the results of the three samples shall be presented by plotting the various model parameters vs. the elongation $\varepsilon = (l - l_o)/l_o$. Here l_o is the initial and l the actual length of the sample. The individual parameter values and its intervals of confidence are plotted as symbols with error bars. The height of the bars is chosen to mark a "2σ"-interval of confidence, assuming the error is normally distributed – that is, the probability to find the true value of the parameter within the interval of confidence is 0.95. Considering the height of the error bars, smooth graphs are drawn through the points evaluated. In general, points showing no error bars have an error smaller than symbol height.

All the length parameters are documented as they come out from the model functions, that is, no corrections according to bending of cylinder surface in radial direction (as proposed in Eq. (8) of [1]) are made. This is approximately equivalent to the assumption of dealing with rectangular block particles instead of cylinders, but the particles volume is a constant.

The variance parameters are plotted (and defined in the fitting program) as relative variances. Thus, for each of both models we plot σ_1/d_1, the relative variance of the cylinder dimensions and σ_2/d_2, the relative variance of the gaps in between.

Because of the fact that the layer lines for all samples and $\varepsilon = 1$ are still somewhat bent, indicating imperfect orientation, it is not strictly allowed to apply our one-dimensional model to these data. Therefore, especially the variance and weight parameters of this elongation should be interpreted cautiously. In the plots they are put in parentheses. Furthermore, bad model adaptation at $\varepsilon = 1$ in any case causes stacking statistics to fit better than the one-dimensional lattice model, even if the actual morphology presents a lattice.

5.2 The main contribution to the fit

The main contribution to the scattering curve is always found to be a superposition of two kinds of fibrils with infinite length but short-range correlation only for both components.

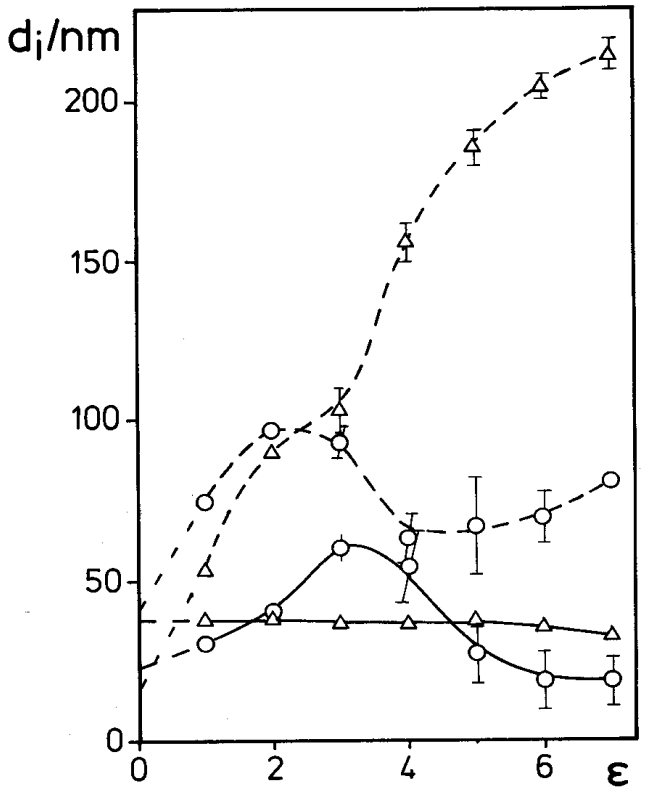

Fig. 4. Dimension parameters d_i vs. elongation ε of pure SBS sample fitted with fibrillar stacking statistics. (○): fibrils with cylinders transversal to drawing direction; (△): fibrils with cylinders orientated in drawing direction. Solid lines: cylinder dimensions (PS); broken lines: gap dimensions (PB)

5.2.1 *Pure SBS*

Figure 4 shows the variation of the distance parameters d_i from the main contribution as a function of elongation. The solid lines can be identified as the dimensions of hard particles, the PS-cylinders. The broken lines describe a weaker phase (the dimensions of which increase considerably with elongation), and thus an identification with the linear dimensions of the PB-matrix in the direction of strain appears to be allowed.

One component is marked by triangles, the other by circles. Let us identify the triangle-marked component with fibrils containing cylinders oriented longitudinally (longitudinal component) and the circle-marked component with fibrils containing cylinders transversal to drawing direction (transversal component). This identification shall be verified by the response of the model components parameters on elongation and variation of the diluent.

Looking at the solid lines (PS-domains) the longitudinal cylinders appear rigid, while if oriented transverse to drawing direction they are weak and extend up to an elongation of $\varepsilon = 3$, where their dimension has increased from 22 nm to 60 nm. After this elongation the transversal system fails, as can be seen from the decrease of the mean radial dimension of the transversal cylinders and the relaxation of the corresponding gap height. The strong increase of the gap in the longitudinal component describes a takeover by this system. An extrapolation to $\varepsilon = 0$ is possible and leads to a cylinder height $h_c = 38$ nm and a diameter $d_c = 23$ nm. The initial heights of the gaps can coarsely be estimated by extrapolating in a plot $d_2(\varepsilon)/(\varepsilon + 1)$ vs. ε for the first three data points. The rough estimates result in an initial gap height of $d_g = 19$ nm for the longitudinal and $d_g = 42$ nm for the transversal component.

The response of the relative variances σ_1/d_1 and σ_2/d_2 to stress for both components is plotted in Fig. 5 and compatible to the explanation given above. At the point of takeover the relative variance of the longitudinal cylinder heights is increased. Concerning the next figure, the reason might be that those cylinders trans-

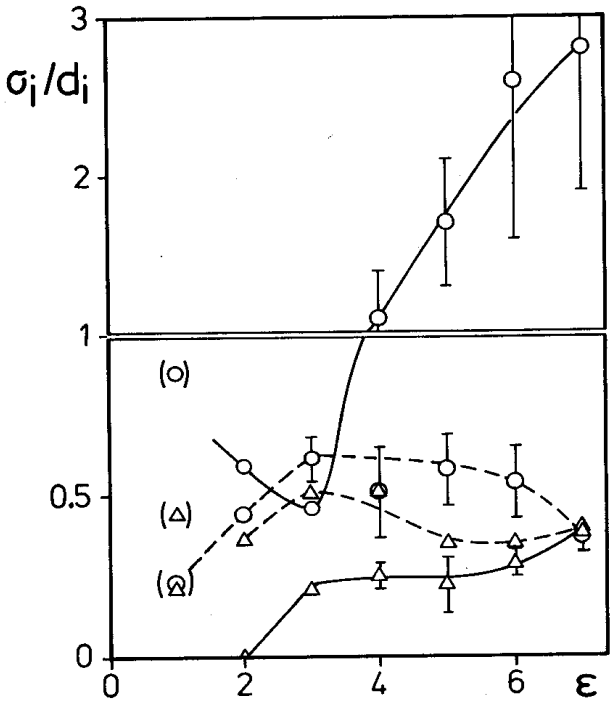

Fig. 5. Relative variances σ_i/d_i vs. elongation ε of pure SBS sample fitted with fibrillar stacking statistics. (○): fibrils with cylinders transversal to drawing direction; (△): fibrils with cylinders orientated in drawing direction. Solid lines: cylinder dimensions (PS); broken lines: gap dimensions (PB). Parentheses for $\varepsilon = 1$ denote poor model adaptation due to bent layer lines

ferred from transversal to longitudinal component between $\varepsilon = 2$ and 3 were not able to orientate perfectly.

The weights A_p of both the longitudinal and transversal components of the scattering under extension are given in Fig. 6. Additionally the weight of the short string component from the subsidiary contribution is dotted. As one can see, the sum of both the weights within the main contribution is nearly constant from $\varepsilon = 3$. At low elongations an orientation effect can be observed. Cylinders orientated indifferently at $\varepsilon = 2$ are comprised in the transversal component, where they result in an increased height variance. At $\varepsilon = 3$ they are orientated in longitudinal direction. In the end, after $\varepsilon = 6$ the transversal component even vanishes by weight. The late increase of the longitudinal component may be due to an increase of $\Delta\varrho$ caused by the formation of holes. In the middle range of ε, however, the postulated plateau for both weights is visible. We recognize that the height of the plateau is the same for both main components and conclude that there seems not to be a preference for the cylinders either to orientate in longitudinal or transversal direction.

We get the best adaption to the measured data if we assume stacking statistics for both components of the main model. From this we deduce that the order of the superstructure is a poor one.

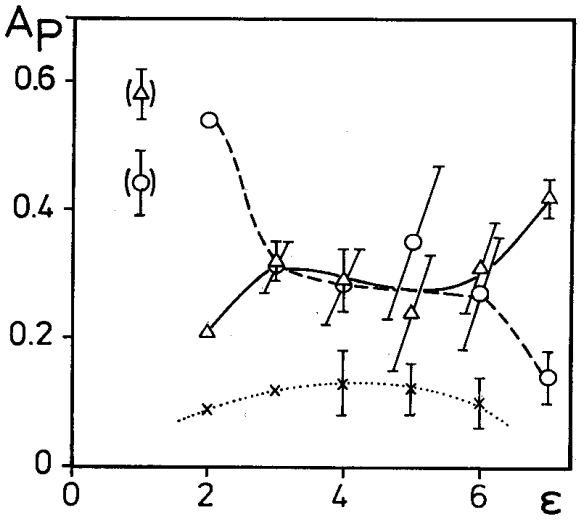

Fig. 6. Weights A_p vs. elongation ε of pure SBS sample fitted with fibrillar stacking statistics. (○): Component of infinite fibrils with cylinders transversal to drawing direction; (△): infinite fibrils with cylinders orientated in drawing direction; (×): finite fibril "short string" component. Parentheses for $\varepsilon = 1$ denote poor model adaptation due to bent layer lines

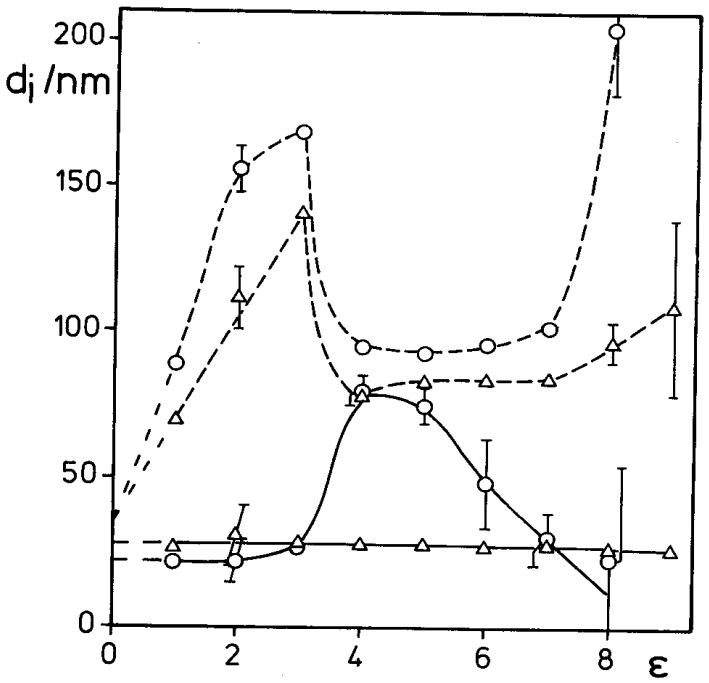

Fig. 7. Dimension parameters d_i vs. elongation ε of P50 sample containing 50 pph of paraffinic oil. (○): Fibrils with cylinders transversal to drawing direction; (△): fibrils with cylinders orientated in drawing direction. Solid lines: cylinder dimensions (PS); broken lines: gap dimensions (PB)

5.2.2 SBS diluted with paraffinic oil

For the sample P50, Fig. 7 shows the dimensions d_i of the main contributions components. As one can see, up to $\varepsilon = 3$ the PS particles of both the longitudinal and the transversal component can be considered as rigid. The extrapolation to $\varepsilon = 0$ yields cylinders of $d_c = 22$ nm and $h_c = 28$ nm. The initial heights of the gaps can be estimated if one plots $d_2(\varepsilon)/(\varepsilon + 1)$ vs. ε for the first three data points and extrapolates towards zero. The coarse estimate results in a gap length of $d_g = 35$ nm for both the longitudinal and the transversal component.

Near $\varepsilon = 4$ the transversal cylinders begin to yield, with the cylinder diameters increasing up to 80 nm. Both the PB-matrix dimensions respond by relaxation to a constant value, further elongation advances by disruption of the cylinders lying crossways to the direction of deformation, until, again, matrix material is elongated after $\varepsilon = 7$.

In Fig. 8 the relative variances σ_i/d_i of the main contribution parameters are shown. There is a sharp peak in the transversal components PS-variance at $\varepsilon = 3$, which can be explained by tension broadening before

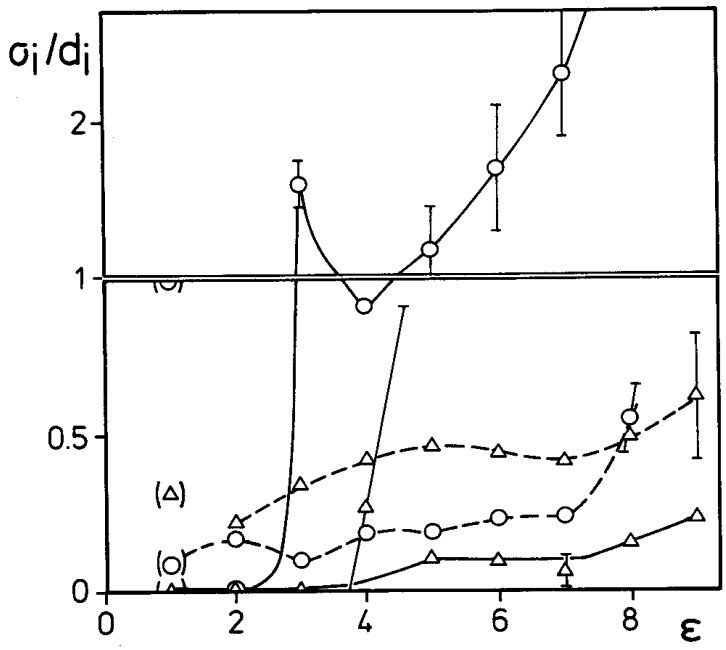

Fig. 8. Relative variances σ_i/d_i vs. elongation ε of P50 sample. (○): Fibrils with cylinders transversal to drawing direction; (△): fibrils with cylinders orientated in drawing direction. Solid lines: cylinder dimensions (PS); broken lines: gap dimensions (PB). Parentheses for $\varepsilon = 1$ denote poor model adaptation due to bent layer lines

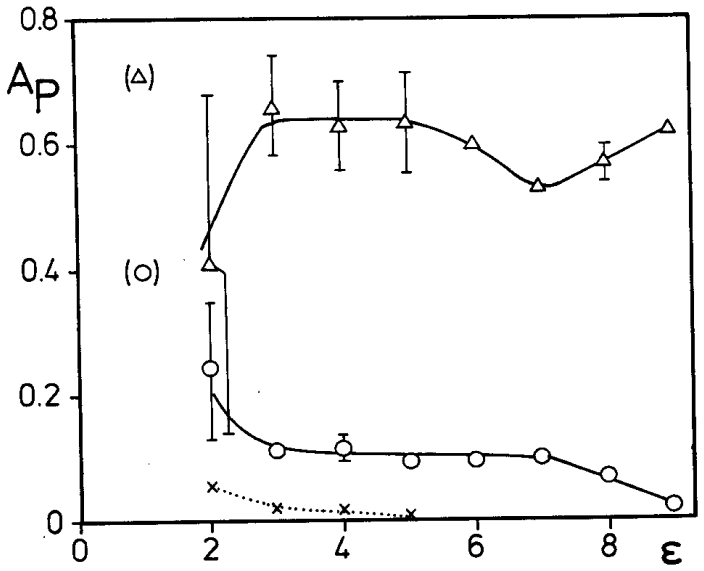

Fig 9. Weights A_p vs. elongation ε of P50 sample. (○): Component of infinite fibrils with cylinders transversal to drawing direction; (△) infinite fibrils with cylinders orientated in drawing direction; (×): finite fibril "short string" component. Parentheses for $\varepsilon = 1$ denote poor model adaptation due to bent layer lines

these cylinders are disrupted. At this elongation the scattering curve is best fitted with a stacking model, which may be explained by the induction of disorder due to the instable state. The following curves again are lattice-model-fitted, but now in the transversal component an inversion of the phase decorating the lattice has taken place. While at $\varepsilon = 2$ the curve is best fitted with a transversal component in which the PS phase is decorating the lattice, from now on the PB matrix forms the decoration. For the longitudinal component no such inversion of lattice decoration is observed. After the yield point of the transversal component there is a similar step in the longitudinal cylinders' variances as that discussed for the SBS sample.

Figure 9 shows the development of the weights A_p as a function of elongation. The initial orientation effect can be observed until $\varepsilon = 3$, where the plateau is reached. Compared with the curves from pure SBS, the amount of the longitudinal component is much higher than that of the transversal one.

Thus, paraffinic oil dilution decreases the cylinders' anisotropy, helps the cylinders to orientate parallel to strain and, in transversal direction, it improves the relative hardness of the cylinders with respect to the matrix. Due to lattice-model-fit the morphology can be said to show a high degree of order.

5.2.3 SBS diluted with aromatic oil

For the sample A50 the response of the distances d_i to stretching is plotted in Fig. 10. The cylinders orientated in the direction of stretching are rigid again. Extrapolation of the cylinder heights will be discussed in the next passage. The transversal cylinders, on the other hand, are flexible even at $\varepsilon = 1$, so that no extrapolation to their initial thickness is possible. A very coarse estimate for the initial cylinder diameter and the gaps can be given the same way as for the preceding samples. The estimate is very coarse, because this time we could only take into account the first two data points. The values are indicated in the plot. The cylinder diameter thus can be estimated by $d_c \simeq 29$ nm and for the gap lengths we get values of $d_g = 19$ nm for the longitudinal and $d_g = 30$ nm for the transversal component.

At $\varepsilon = 5$ the transversal system has failed and one finds a takeover by the longitudinal system, indicated by a sudden increase of the PB mean extension. A similar behavior was found in the undiluted SBS sample at an elongation of $\varepsilon = 4$.

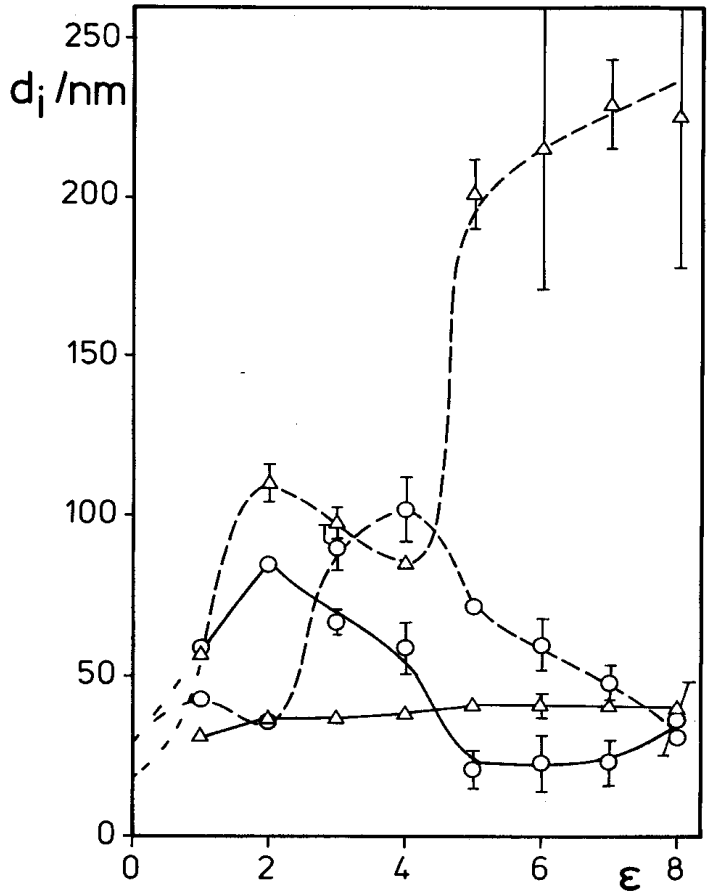

Fig. 10. Dimension parameters d_i vs. elongation ε of A50 sample fitted with fibrillar stacking statistics. (O): Fibrils with cylinders transversal to drawing direction; (Δ) fibrils with cylinders orientated in drawing direction. Solid lines: cylinder dimensions (PS); broken lines: gap dimensions (PB)

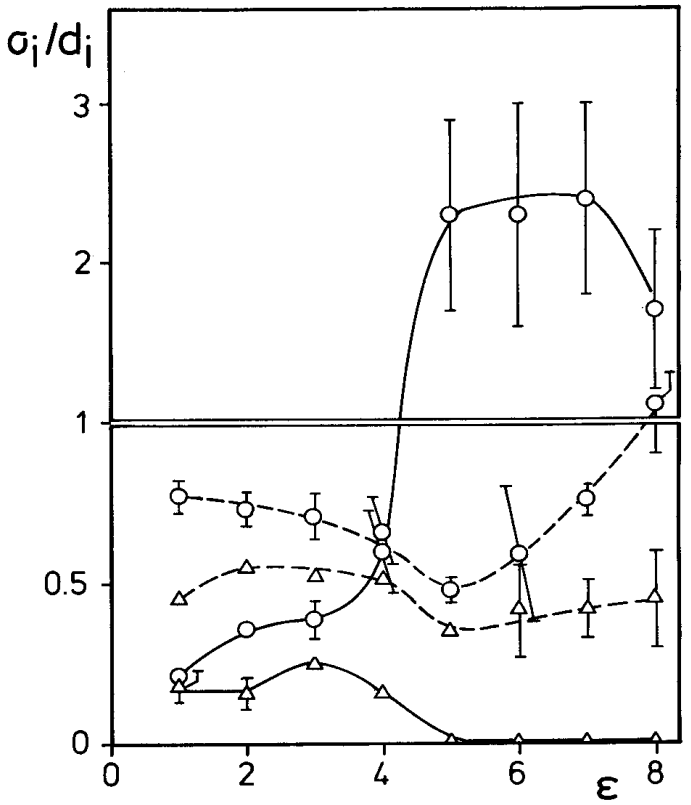

Fig. 11. Relative variances σ_i/d_i vs. elongation ε of A50 sample fitted with fibrillar stacking statistics. (O): Fibrils with cylinders transversal to drawing direction; (Δ): fibrils with cylinders orientated in drawing direction. Solid lines: cylinder dimensions (PS); broken lines: gap dimensions (PB). Parentheses for $\varepsilon = 1$ denote poor model adaptation due to bent layer lines

In Fig. 11 the curves of the relative distance variances σ_i/d_i of the A50 sample are shown. Transversal cylinder disruption is indicated by the known increase of the curve.

The relative variances of the longitudinal component show a new behavior. For low elongations the cylinder heights are subject to an uncertainty, while from $\varepsilon = 5$ they are not. This effect can be explained by assuming imperfect orientation for low elongations that improves for $\varepsilon > 4$, accompanied by an increase of the effective cylinder height towards the true initial value. In fact this behavior can be observed in Fig. 10. Thus for the initial mean cylinder height we find $h_c =$ 41 nm. This explanation is supported by the response of the longitudinal components PB gaps. Those gaps in the range of $\varepsilon = 2 \ldots 4$ show a significant relaxation behavior, before the longitudinal component takes over.

In Fig. 12 the weights A_p of the sample A50 are plotted. As one can see, the plateau is reached lately at $\varepsilon = 5$. Here the amount of the longitudinal component is very low while most of the cylinders contribute to the transversal component. At $\varepsilon = 3$ there is a significant valley in the transversal component that is accompanied by a peak in the longitudinal component. The peak coincides with the range of longitudinal fibril relaxation and the valley does so with the range of transversal cylinder disruption. This phenomenon might be caused by an uneven oil distribution between the matrix of the longitudinal and that of the transversal component. If that were true, the relaxing longitudinal gaps would have to be able to expel the aromatic oil, while the oil would have to be enriched in the transversal components gaps. A phenomenon of uneven oil distribution between the components would not be observable for paraffinic oil dilution, because for that diluent there is no contrast between the electron

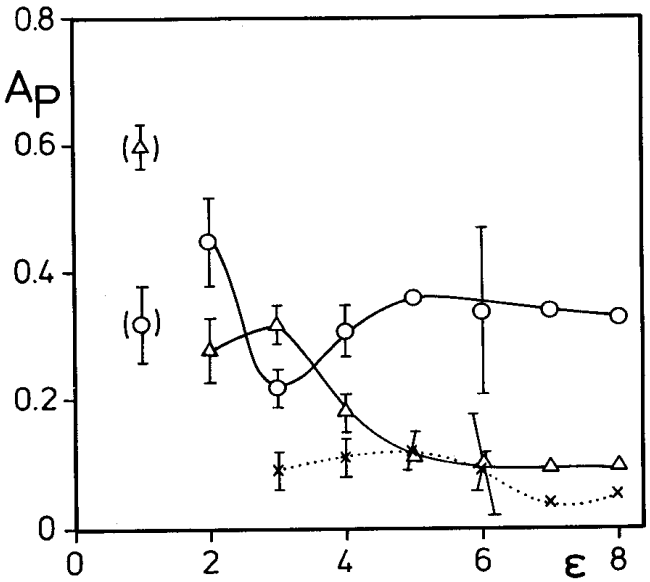

Fig. 12. Weights A_p vs. elongation ε of A50 sample. (O): Component of infinite fibrils with cylinders transversal to drawing direction; (Δ): infinite fibrils with cylinders orientated in drawing direction; (×): finite fibril "short string" component. Parentheses for $\varepsilon = 1$ denote poor model adaptation due to bent layer lines

densities of the PB matrix and that of the oil [9]. Yet, an explanation by an orientation phenomenon seems more probable to us, because it fits well to the descriptions of the preceding two figures. So we assume that the increase of the longitudinal components amount is caused by a latent (and only fair) longitudinal orientation of a certain amount of cylinders at low elongations, so that the longitudinal component is increased. While transversal cylinders under tension are disrupting, an orientation relaxation from longitudinal to transversal orientation occurs, which can be observed by the decrease of the longitudinal component and a corresponding increase of the transversal component between $\varepsilon = 3$ and 5.

Thus, aromatic oil dilution slightly increases the cylinders' height, hinders the cylinders' optimal orientation parallel to stress and reduces the relative hardness of the cylinders transversal to drawing direction. The morphology shows a low degree of order, as is observed for the undiluted SBS.

5.3 The subsidiary contribution

As discussed before, the evidence of the finite-fibril components is a rather weak one. In spite of this the results shall be documented in the following. The shorter string component shows a rather stable

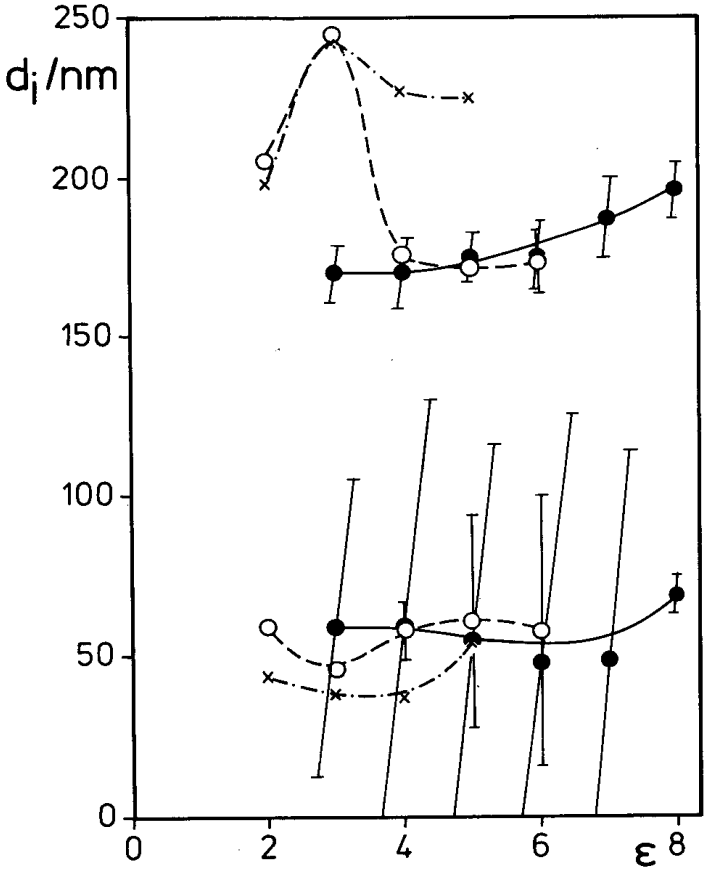

Fig. 13. String lengths (above) and PS head heights of the "short string component" d_i vs. elongation ε. (O) Pure SBS; (×) P50 sample; (●) A50 sample

amount over a long range of elongations. Its string length is between 170 nm and 250 nm, and its weights A_p have been plotted in Figs. 6, 9, and 12. Figure 13 shows a plot of the string lengths (upper curves) and the heights of the heads for all three samples (beneath). Open circles mark the pure SBS, filled circles the A50 sample, and x-marks are used for the P50 sample. As one can see, the height of the PS heads is about 50 nm for all samples and all elongations. Their intervals of confidence are wide for A50 in general and for SBS at high elongations. The string lengths, on the other hand, can be determined with good significance. SBS and P50 show a peak at $\varepsilon = 3$, with a maximum height of about 250 nm, A50 a steady increase as a function of ε from 170 nm at $\varepsilon = 3$ to 200 nm at $\varepsilon = 8$. The relative variances of the strings always were iterated towards zero, so these parameters have to be removed from the model function. For the PS heads, Fig. 14 documents the relative variances. Here the wide error bars are

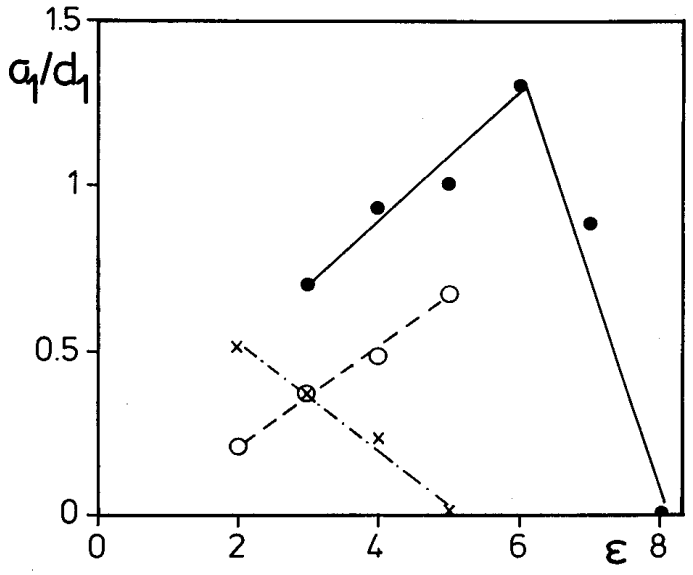

Fig. 14. Relative variances σ_1/d_1 of PS heads in the "short string component" vs. elongation ε. (O) Pure SBS; (×) P50 sample; (●) A50 sample. Poor intervals of confidence are not plotted

omitted for clarity. Because of the error bars width a discussion of the trend seems unappropriate.

A second string component with a string-length parameter of about 500 nm only is found in the scattering curves of the oil diluted samples at elongations of $\varepsilon = 2$ and 3. The parameters of these fits are shown in Table 1. As one can see, only the string lengths and their relative variances show significant values.

Thus, even if we assume the principal correctness of superposed finite fibrils for the samples superstructure, we have to be very cautious with interpretation. In fact, the parameters that are produced by the regression procedure are not unreasonable. The long-string component could be produced by PB chains in the oil-diluted samples that are fully extended. An estimation of chain length with the PB chain being statistically composed [13] from equal parts of 1,2-butadiene and 1,4-butadiene monomer units is in fair agreement with the length of 500 nm. It is obvious that oil dilution will reduce the entanglements of the PB chains, so that we could explain the absence missing of the long-string component in the undiluted samples' scattering. The most simple explanation for the short-string component could be the assumption of a chain without entanglements running through the neighboring cylinder particle and folding back to the original cylinder. This would explain a mean string length of about 250 nm that is reached as the maximum for the samples SBS and P50. The variation of string length as a function of elongation, on the other hand, shows that a more complex explanation is needed to understand the behavior of this component.

Table 1. Resulting parameters of the long-string component fitted to the scattering curves of oil-diluted SBS samples P50 and A50

Sample	Parameter	$\varepsilon = 2$	$\varepsilon = 3$
P50	A_p	0.17 ± 0.36	0.090 ± 0.050
	d_1/nm	29.00 ± 35.00	8.000 ± 21.000
	d_2/nm	489.00 ± 28.00	500.000 ± 60.000
	σ_1/d_1	0.20 ± 25.00	0.300 ± 1.400
	σ_2/d_2	0.08 ± 0.01	0.04 ± 0.020
A50	A_p		0.003 ± 0.002
	d_1/nm		20.000 ± 67.000
	d_2/nm		499.000 ± 44.000
	σ_1/d_1		0.400 ± 0.500
	σ_2/d_2		0.0

5.4 *Discussion of dimension extrapolations and estimates*

In the preceding paragraphs we could extrapolate or estimate values for the mean dimensions of the particles and the mean distances between them for the undrawn state, compiled in Table 2.

As one can see, pure SBS shows a very wide gap d_{gc} in transversal direction between neighboring cylinders. We interpret this as an effect of bad phase separation (cf. [9]). Imperfect PS particles between the more stable cylinders even vanish at a very low elongation. Therefore, in d_{gc} we estimate the mean distance between two stable cylinders with an imperfect particle in between.

Paraffinic oil dilution only affects the cylinders heights, while aromatic oil dilution mainly seems to influence the cylinders' diameters. Both diluents cause a reduction of the h_c/d_c-ratio of the cylinders, but paraf-

Table 2. Extrapolated or estimated (*) values for the cylinder dimensions and the distances in between for the undrawn state. h_c, d_c: cylinder height and diameter. d_{gl}, d_{gc}: gaps in longitudinal and transversal direction (with respect to the cylinder axis)

	SBS	P50	A50
h_c/nm	38	28	41
d_c/nm	23	22	*29
d_{gl}/nm	*19	*35	*19
d_{gc}/nm	*42	*35	*30

finic oil dilution decreases the cylinder height, while aromatic oil dilution seems to increase the cylinder diameter.

If we trust in the estimated values for the mean initial distances between the cylinder edges, the result on the particle dimensions can even be generalized. From the values in Table 2 we construct nearly the same "pseudo lattice cell" for P50 and A50 (see Fig. 15), but the lattice cell of pure SBS appears somewhat wider in transversal cylinder direction. A result compatible with this was found in a preceding work on the unstretched samples: a long period nearly constant for three kinds of diluents and oil dilutions up to 140 pph [9].

Thus, a reason for the different amount of cylinders allotted to each of the two components with different cylinder orientation is apparently induced by topology: the cylindrical particles' dimensions within a pseudo lattice cell of nearly constant extent, determining the particles' possibility to rotate and follow an external torque.

5.5 *General discussion of the weights A_p*

Considering the changes of A_p as a function of elongation, the assumption of constant contrast $\Delta\varrho_{el}$ and constant number of cylinders n does not hold even in the beginning part of the curves. Otherwise, the sum $A_{Ps}(\varepsilon) = A_{P||}(\varepsilon) + f \cdot A_{P\perp}(\varepsilon)$ for the longitudinal and the transversal component should not be a function of ε. Here f is the additional attenuation factor for fibrils with cylinders transversal to drawing direction, taken into account because of our offset section to the scattering pattern. Determination of f from two optional pairs of weight values does not result in a constant value for each sample, yet f sometimes turns out to be greater than 1 or is even negative.

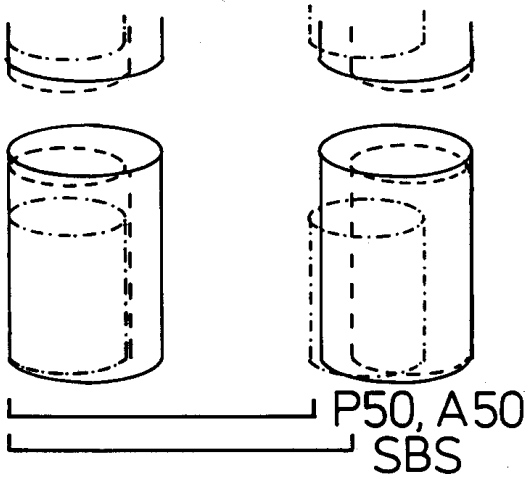

Fig. 15. Pseudo lattice cells containing cylindrical particles constructed from extrapolated or estimated dimensions for the undrawn state. Broken line: pure SBS; dashed and dotted line: sample P50, 50 pph paraffinic oil dilution; solid line: A50, 50 pph aromatic oil dilution. Decrease of lattice constants transversal component on oil dilution is indicated below

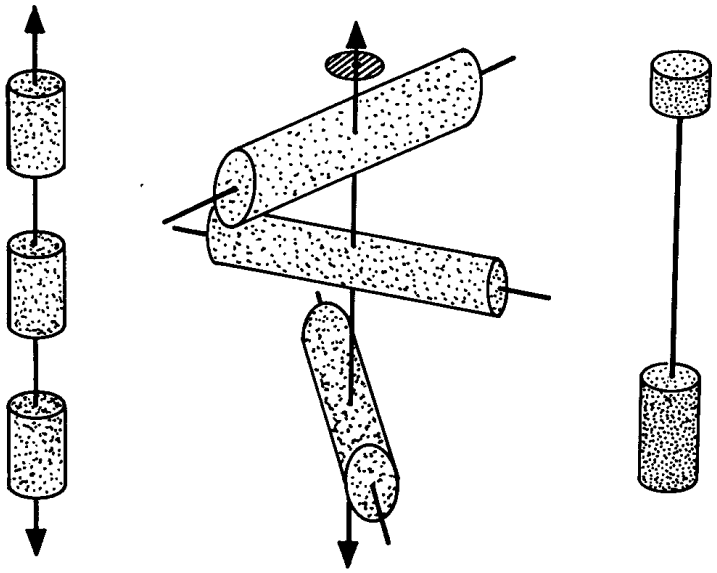

Fig. 16. Illustrations of longitudinal (on the left) and transversal (in the middle) component fibrils. Transversal component fibril shows the general case without correlation of orientation among the cylinders in the fibril. The effective correlated surface of the cylinders S_{cc} is indicated above the fibril. A model string is shown on the right side, the different heights of its PS-heads indicating the extreme variance of the extension of these heads

One the other hand, a plateau in both the A_P components can be found for every sample within a certain range of mean elongation. As mentioned before, the assumption of constant contrast and constant number of cylinders could probably hold for this range of elongation. So if we want to quantify the relative amounts of orientatable cylinders, we can assume $f = 1$, which means that the correlated surface S_{cc} in stretching direction, even for fibrils containing transversal cylinders, is just given by the cylinder diameter (Fig. 16, middle). The other limiting case is that of perfect correlation of orientation among cylinders belonging to the same fibril, in which we can estimate f from the cylinder height, the distance of offset to our section s'_{12}, and the plot in Fig. 1.

Considering the simpler disordered case, we find that for the samples SBS, 50%, P50, 87%, and A50,

21 %, of the cylinders are orientated parallel to drawing direction in the plateau region.

So one can see that the general trend of the sum of the weights A_{P_S} is not contrary to the trend that was found in earlier work [9], namely that paraffinic oil dilution improves phase separation, while diluting with 50 pph of aromatic oil decreases the contrast due to the high electron density of the aromatic oil.

6. Conclusions

The results of this work show that the use of an adapted theoretical approach and model for the evaluation of the small angle x-ray scattering data can give profound information on the two-phase topology of an (oil diluted) SBS block copolymer, and not only in the drawn state. Since the scattering curves are determined by the particles' structural factor, no Porod law can be found above the level of statistical noise. Thus, an analysis of topological parameters in real space after Fourier transform, as proposed by Ruland in his theory of interface distribution [11] is impossible, and we need to evaluate the parameters in a regression analysis directly on the measured data set.

The disadvantage of this method is that structural parameters are not obviously revealed, as they are in an interface distribution. Thus, one has to be very cautious in fitting models to the scattering curve. The way that was chosen here is that of confining the model function step by step, beginning with a very general one. Decisions on the next step of confinement are supported by considerations about the physical sense of the output parameters and estimates on the quality of fits, as can be found in the theory of nonlinear regression analysis.

The advantage of the method is that it has the possibility to compute estimated intervals of confidence for every parameter found, due to the direct fit on unsmoothed scattering curves.

Lately our efforts to get electron micrographs from our samples resulted in the first pictures showing contrast, so that we were able to compare our results with electron microscopy in a following paper.

Acknowledgements

The authors are indebted to Dr. R. Bordeianu and Dipl. Eng. P. Ghioca from the Chemical Research Institute ICECHIM, Bucharest, Romania, for sample preparation and valuable discussions. We also thank Prof. Zachmann for valuable discussions.

Development of the SIT-Vidicon-system was funded by BMFT, the German Federal Ministry for Research and Technology under contract number 05305HXB.

References

1. Stribeck N (1989) Colloid Polym Sci 267:301-310
2. Hendus H, Illers K-H, Ropte E (1967) Colloid Polym Sci 216:110-119
3. Séguéla R, Prud'homme J (1988) Macromolecules 21:635-643
4. Pakula T, Saijo K, Kawai H, Hashimoto T (1985) Macromolecules 18:1294-1302
5. Richards RW, Mullin JT (1988) Mat Res Soc Symp Proc 79:299-308
6. Bordeianu R, Cerchez I, Ghioca P, Stancu R, Buzdugan E (1986) In: Ceausescu E (ed) Forschungen im Bereich der Chemie und Technologie der Polymere. Birkhäuser, Basel pp 65–77
7. Ceausescu E, Bordeianu R, Ghioca P, Cerchez I, Buzdugan E, Stancu R (1983) Rev Roumaine de Chimie 28:299–323
8. Ceausescu E, Bordeianu R, Ghioca P, Buzdugan E, Stancu R, Cerchez I (1984) Pure & Appl Chem 56:319–328
9. Polizzi S, Stribeck N, Zachmann HG, Bordeianu R (1989) Colloid Polym Sci 267:281-291
10. Polizzi S, Bösecke P, Stribeck N, Zachmann HG, Zietz R, Bordeianu R (1988) to be submitted to Polymer
11. Ruland W (1977) Colloid Polym Sci 255:417–427
12. Draper NR, Smith H (1966) Applied Regression Analysis. John Wiley, New York, chap 10, pp 263–306
13. Bordeianu R, private communication

Received September 19, 1988;
accepted March 2, 1989

Authors' address:

Dr. N. Stribeck
Institut TMC
Bundesstraße 45
D-2000 Hamburg 13, F.R.G.